Final Report

Final Report - DOE-Stanford-115503

Project Title:	"Perovskite Solar Cells for High-Efficiency Tandems"
Project Period:	July 1, 2014 to Sep 30, 2017
Submission Date:	September 30, 2017
Recipient:	Stanford University
Address:	476 Lomita Mall Stanford, CA 94305
Website (if available)	N.A.
Award Number:	DE-EE0006707
Working Partners:	Massachusetts Institute of Technology
Cost-Sharing Partners:	Massachusetts Institute of Technology
PI:	Michael McGehee Professor Phone: 650-736-0307 Fax: 650-498-5596 Email: mmcgehee@stanford.edu
DOE Project Team:	DOE Contracting Officer Diana Bobo DOE Project Officer Lenny Tinker DOE FOA Manager RoseMarie Holsing

Michael D McGehee September 30, 2017

_____

Signature Date

Executive Summary:

In the first year of the project, we made the first monolithic two-terminal perovskite-silicon tandem solar cell. While our paper only reported an efficiency of 13.7%, it sparked international interest in making these kinds of tandems and provided a list of what needed to be done to improve the efficiency. At the end of the second year of the project, we made a second-generation tandem with the perovskite cell inverted and placed on top of a heterojunction silicon solar cell. The efficiency leapt up to a new NREL-certified world record of 23.6% that still stands as the best for the class of solar cells.

At every stage in the project, we emphasized the importance of improving stability just as much as raising the efficiency. We were one of five groups that announced around the same time that replacing methylammonium with a combination of cesium and formamidinium substantially improves thermal stability. We were the first to show how to use either metal oxide nanoparticles or ALD tin oxide as a buffer layer to enable the sputtering of ITO. The ITO dramatically improves stability of perovskite solar cells by preventing thermal decomposition and keeping oxygen and moisture out. It also is far less prone to react with halogens than the metals that most perovskite researchers use. We packaged the solar cells and passed the IEC 1000 hour 85°C-85% humidity damp heat test. We now have an excellent infrastructure in place for characterizing the stability of dozens of perovskite solar cells at elevated temperatures under illumination.

Our project has successfully inspired many researchers to join us in the quest to make stable tandems with 30% efficiency that could be manufactured cost-effectively. We have published in *Nature Energy* and been invited to write a review article for the same journal. A feature news article on the project was written by Robert Service for *Science*. The project has been alluded to in *The Economist* and *Consumer Reports*. We have also been invited to write a review article on our stability research in a special issue on perovskite solar cells in *Chemical Reviews*. We have received many invitations to speak at conferences. Prof. McGehee gave a keynote lecture at the IEEE Photovoltaic Specialists Conference in June 2017. We have also presented our research in webinars with the Materials Research Society and the Stanford Center for Professional Development that were each attended by more than 300 people. Companies that have requested meetings with us to talk about the research include First Solar, SunPower, DuPont, Tesla, Exxon, EPRI, Oxford PV, BASF, Hunt Energy, Schlumberger and Total.

Table of Contents

To be written just before final submission

Background

Tandems, *i.e.*, multijunction solar cells, currently comprise the only commercially mature technology for achieving power conversion efficiencies exceeding the Shockley-Queisser limit. Today, high-efficiency commercial tandem solar cells are exceedingly

expensive, as they are made by growing films of III-V semiconductors epitaxially on single-crystal wafers.

The efficiency and understanding of perovskite solar cell has advanced at an astounding rate since 2012, surpassing 22% in 2016, despite only a five years of study as a solar cell material. Devices exceeding 15% efficiency have been achieved both with solution and vapor-phase deposition of the perovskite material onto inexpensive glass substrates, and could potentially be manufactured at low cost and high throughput. The bandgap of $APb(Br_xI_{1-x})_3$ (A= CH_3NH_3, $CH(NH_2)_2$, or Cs; x = 0 to 1) can be tuned from 1.5 eV to 2.3 eV by substituting iodide with bromide or by varying the cation A. This range of bandgaps is well suited for making a tandem solar cell using a conventional silicon solar cell as the low bandgap junction. Furthermore, the record published devices have a short circuit current density (J_{SC}) of over 21 mA/cm^2, which could be current-matched to a silicon cell in a tandem device. These devices also achieve remarkably large open circuit voltages (V_{OC}) of over 1.1 V from a 1.6 eV bandgap polycrystalline material. These attributes make hybrid perovskites an attractive candidate material for the large bandgap absorber of a tandem solar cell with silicon.

Integration of perovskites with silicon photovoltaics to make monolithic tandem solar cells presents numerous engineering challenges that had not been previously investigated by the photovoltaics community. Firstly, the perovskite junction needs to be semitransparent to allow light to reach the silicon solar cell. This requires a means for depositing the semitransparent electrodes on top of the perovskite without degrading the perovskite with high temperature processing steps or solvents. Furthermore, conventional perovskite solar cells are made using a superstrate architecture and need to be adapted to work with a silicon substrate configuration. Secondly, a carrier selective recombination junction between the silicon and perovskite devices needs to be developed. Thirdly, reflections at interfaces in the tandem device structure need to be carefully managed. This optimization problem is challenging as strategies such as front surface texturing of the silicon solar cell are not compatible with solution deposition of the perovskite solar cell. Lastly, the stability of perovskite modules to moisture, light, electrical bias and other stressors needs to greatly improve so that the tandem modules can have lifetimes of 30 years or more.

The project objectives stated in the grant proposal were to model, design, fabricate and optimize perovskite-silicon tandem solar cells with an expected power conversion efficiency of 25% in a current-matched perovskite-silicon tandem. We set out to identify the primary degradation mechanism of perovskite solar cells and design encapsulation approaches to enable reliable devices.

During Year 1, we had the goal of developing the individual components that would be integrated into current-matched silicon-perovskite tandem solar cell in Year 2. We set out to improve the film quality and engineer the contacts in order to demonstrate the first substrate perovskite devices. We planned to design and fabricate the crystalline silicon bottom cell, design and fabricate the tunnel junction, and the silicon-titania interface that will connect the silicon and perovskite junctions. In Year 2, we planned to put the pieces together to build a two-terminal (2T) silicon-perovskite tandem while continuing to improve the perovskite device electrodes. We set out to determine the primary degradation pathways of perovskite devices and encapsulation requirements to improve device

stability. We expected to achieve 20% efficient two-terminal perovskite-silicon tandems at the end of Year 2. In Year 3, we the goals were to optimize the silicon-perovskite device and develop encapsulation methods to promote the lifetimes of these devices to achieve 25% efficient current matched perovskite-silicon tandems.

Introduction:

The first monolithic perovskite/silicon tandem was made with a diffused silicon *p*-*n* junction, a tunnel junction made of n^{++} hydrogenated amorphous silicon, a titania electron transport layer, a methylammonium lead iodide absorber, and a Spiro-OMeTAD hole transport layer (HTL)[8]. The power conversion efficiency (PCE) was only 13.7% due to excessive parasitic absorption of light in the HTL, limiting the matched current density to 11.5 mA/cm^2. Werner *et al*.[15] raised the PCE to a record 21.2% by switching to a silicon heterojunction bottom cell and carefully tuning layer thicknesses to achieve lower optical loss and a higher current density of 15.9 mA/cm^2. It is clear from these reports that minimizing parasitic absorption in the window layers is crucial to achieving higher current densities and efficiencies in monolithic tandems. To this end, the window layers through which light first passes before entering the perovskite and silicon absorber materials must be highly transparent. The front electrode must also be conductive to carry current laterally across the top of the device. Indium tin oxide (ITO) is widely utilized as a transparent electrode in optoelectronic devices such as flat-panel displays, smart windows, organic light-emitting diodes, and solar cells due to its high conductivity and broadband transparency[21]. ITO is typically deposited through magnetron sputtering; however, the high kinetic energy of sputtered particles can damage underlying layers[22]. In perovskite solar cells, a sputter buffer layer is required to protect the perovskite and organic carrier extraction layers from damage during sputter deposition. The ideal buffer layer should also be energetically well aligned so as to act as a carrier-selective contact, have a wide bandgap to enable high optical transmission, and have no reaction with the halides in the perovskite. Additionally, this buffer layer should act as a diffusion barrier layer to prevent both organic cation evolution and moisture penetration to overcome the often-reported thermal and environmental instability of metal halide perovskites[23]. Previous perovskite-containing tandems utilized molybdenum oxide (MoO_x) as a sputter buffer layer[9,11,12], but this has raised concerns over long-term stability, as the iodide in the perovskite can chemically react with MoO_x[24].

Mixed-cation perovskite solar cells have consistently outperformed their single-cation counterparts. The first perovskite device to exceed 20% PCE was fabricated with a mixture of methylammonium (MA) and formamidinium (FA)[25]. Recent reports have shown promising results with the introduction of cesium mixtures, enabling high efficiencies with improved photo-, moisture, and thermal stability[26–30]. The increased moisture and thermal stability are especially important as they broaden the parameter space for processing on top of the perovskite, enabling the deposition of metal oxide contacts through atomic layer deposition[31,32] (ALD) or chemical vapor deposition (CVD) that may require elevated temperatures or water as a counter reagent. Both titanium dioxide (TiO_2) and tin oxide (SnO_2) have consistently proven to be effective electron-selective contacts for perovskite solar cells and both can be deposited via ALD at temperatures below 150 °C[33–35].

Project Results and Discussion:

We introduced a bilayer of SnO_2 and zinc tin oxide (ZTO) that can be deposited by either low-temperature ALD or pulsed-CVD as a window layer with minimal parasitic absorption, efficient electron extraction, and sufficient buffer properties to prevent the organic and perovskite layers from damage during the subsequent sputter deposition of a transparent ITO electrode. We explored pulsed-CVD as a modified ALD process with a continual, rather than purely step-wise, growth component in order to considerably reduce the process time of the SnO_2 deposition process and minimize potential perovskite degradation. These layers, when used in an excellent mixed-cation perovskite solar cell atop a silicon solar cell tuned to the infrared spectrum, enable highly efficient perovskite-silicon tandem solar cells with enhanced thermal and environmental stability.

Single-Junction Perovskite Solar Cells

We first fabricated single-junction perovskite solar cells on ITO-coated glass in order to develop a transferrable architecture for monolithic tandem solar cells on silicon. We fabricated the $Cs_{0.17}FA_{0.83}Pb(Br_{0.17}I_{0.83})_3$ (CsFA) perovskite top cell, with a bandgap of 1.63 eV (Supplementary Figure 1), in the *p-i-n* architecture, in which the electron-selective contact is deposited on top of the perovskite absorber layer and acts as a window layer. Suitable contacts for this geometry include *n*-type metal oxides such as zinc oxide (ZnO), TiO_2, and SnO_2. Figure 1a displays a schematic of the device structure. The perovskite was deposited on top of nickel oxide (NiO_x)—a hole-selective contact—to achieve higher voltage and stability than with the traditional poly(3,4-ethlenedioxythiophene) polystyrene sulfonate (PEDOT:PSS) contact[36,37]. The CsFA perovskite was deposited from a stoichiometric solution containing CsI, formamidinium iodide (FAI), PbI_2, and $PbBr_2$ in a mixture of dimethylformamide (DMF) and dimethyl sulfoxide (DMSO). This deposition method was modified from that of Chenyi *et al*.[27] and the full details of device fabrication are provided in the Methods section.

To deposit an electron-selective contact, we attempted to use phenyl-C61-butyric acid methyl ester (PCBM) and aluminum-doped zinc oxide (AZO) nanoparticles, which were previously used successfully in a methylammonium lead iodide ($MAPbI_3$) perovskite solar cell[38]; however, the devices were largely shunted due to the high surface roughness of the CsFA perovskite (Supplementary Figure 2). Spin coating on rough surfaces requires thick, planarizing layers to be applied to prevent shunt pathways, leading to lower optical transmission (Supplementary Figure 2). Evaporation, ALD, and CVD enable the fabrication of uniform, conformal, thin films offering high optical transmission, regardless of surface texture. SnO_2 can be deposited by ALD using tetrakis(dimethylamino)tin(IV) (TDMASn) and water at temperatures as low as 30 °C[39], although deposition temperature is known to affect the stoichiometry and electronic properties of metal oxide films[40]. We use this ALD system at 100 °C to deposit SnO_2. Others have shown that a thin layer of PCBM between SnO_2 and the perovskite increases efficiency[29]. We thermally evaporated 1 nm of LiF and 10 nm of PCBM to leverage their good electron extraction properties (Supplementary Figure 3), while still achieving high optical transmission. We find that LiF acts as a shunt blocking layer similar to how thin, insulating, silicon oxide layers have been employed previously in thin-film silicon solar cells to block shunt pathways and

increase fill factor (*FF*)[41]. We believe LiF helps enable us to fabricate our 1 cm^2 aperture area tandems without a loss in *FF* and a large spread in efficiency (see Supplementary Figure 9). Additionally, we note that PCBM thermally decomposes during evaporation to a more thermally stable isomer with very similar electronic properties[42].

On top of the PCBM layer, we deposited 4 nm of SnO_2 by ALD at 100 °C, followed by 2 nm of ZTO. The X-ray photoelectron spectroscopy (XPS) sputter depth profile of the 4 nm SnO_2/2 nm ZTO stack in Supplementary Figure 4 shows only partial diffusion of zinc into the tin oxide film, indicating that 4 nm of SnO_2 is sufficient to prevent detectable concentrations of zinc from reaching the perovskite. ZTO was deposited by combining SnO_2 and ZnO ALD processes in a repeating supercycle consisting of three cycles of SnO_2 followed by three cycles of ZnO[43,44]. The parameters for the individual SnO_2 and ZnO processes used in the ZTO supercycle are described in Supplementary Tables 1-4. This process resulted in an effective growth rate of 5.8 Å/supercycle, or 0.1 nm/min. We investigated faster processing methods of our window layer by reducing the purge time from 30 sec to 5 sec between pulses. In doing so, the process approached the pulsed-CVD growth regime, further increasing the deposition rate to 0.5 nm/min, resulting in a total window layer deposition time of approximately 15 min. Current-voltage (*J-V*) and XPS data in Supplementary Figures 5 and 6 illustrate the identical performance and stoichiometry of SnO_2 and ZTO layers deposited via ALD and pulsed-CVD. Pulsed-CVD was used in the fabrication of our champion devices, which is noteworthy as CVD has the potential to reduce processing time compared to ALD and minimize thermal-induced degradation during processing.

A 150-nm-thick ITO electrode with a sheet resistance of 30 Ω/□ was sputtered on top of the cell, as in our previous work[38]. Optical modelling of the device stack indicated that thicker ITO layers introduce significant current losses through parasitic absorption (Supplementary Figure 7) while thinner layers reduce *FF* due to high series resistance. The 2 nm of ZTO is necessary to achieve low contact resistance with ITO and reach a high *FF*, as shown in Supplementary Figure 3. Finally, we finished the device stack with an evaporated silver metal electrode around the perimeter of the 1 cm^2 device area to minimize series resistance and a 150-nm-thick, thermally evaporated LiF antireflection coating.

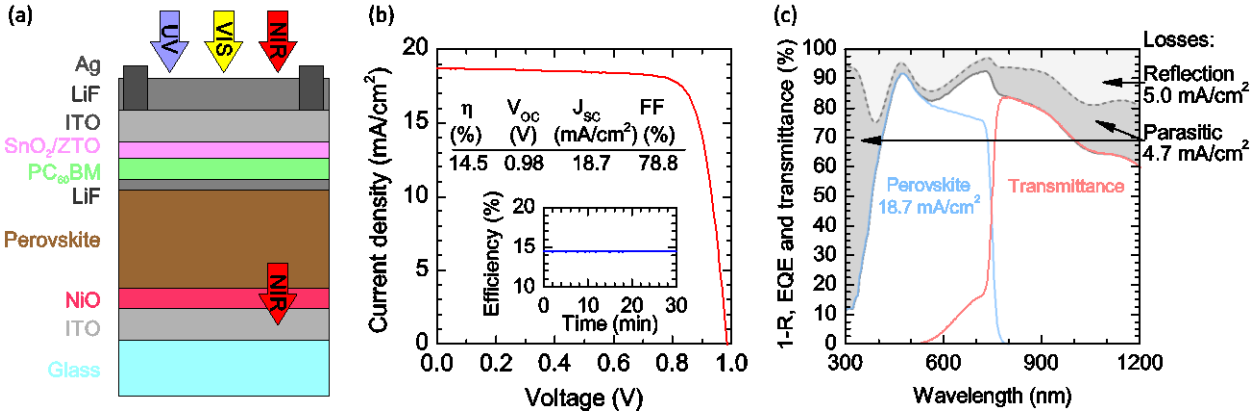

Figure 1. Design and performance of the perovskite top cell. (a) Schematic of the single-junction, semi-transparent perovskite solar cell (not to scale), (b) J-V curve and efficiency at the maximum power point (inset) of the perovskite solar cell with

illumination through the SnO_2 side, (c) total absorbance (1-R, where R is the reflectance; dashed grey line), EQE (solid blue line), and transmittance (solid red line) of the perovskite solar cell. The sum of the EQE and transmittance (solid grey line) is the total summed current density available to be captured in the final tandem. The light and dark grey shaded areas represent the light lost to reflection and parasitic absorption, respectively, and the associated current density losses are indicated.

The equivalent efficiency of the semi-transparent and opaque devices speaks to the efficacy of the SnO_2/ZTO bilayer and sputtered ITO layer as an electron-selective contact. Additionally, the high *FF* of 78.8% and lack of an extraction barrier, demonstrated by the *J*-*V* curve in Figure 1b, indicate that the bilayer is a successful sputter buffer layer. Figure 1c shows the external quantum efficiency (EQE), transmittance, and 1-reflectance measured from the SnO_2/ZTO bilayer (front) side. The high EQE, with an integrated current density of 18.7 mA/cm^2, and low parasitic losses between 400 and 750 nm showcase the optical properties of the bilayer and sputtered ITO. The AM1.5G-weighted average transmittance of this device between the perovskite bandgap at 765 nm and the silicon bandgap at 1200 nm is 74%. Figure 1b indicates that there is still room for open-circuit voltage (V_{OC}) improvement, as the bandgap-voltage offset is over 0.65 V. We believe that the origin of the voltage loss is primarily due to the difficultly in crystallizing the CsFA perovskite in the inverted architecture on a planar surface. Supplementary Figure 2 reveals considerable surface roughness, which may cause voids in the LiF and PCBM layers during the evaporation.

Two-Terminal Tandem Solar Cells

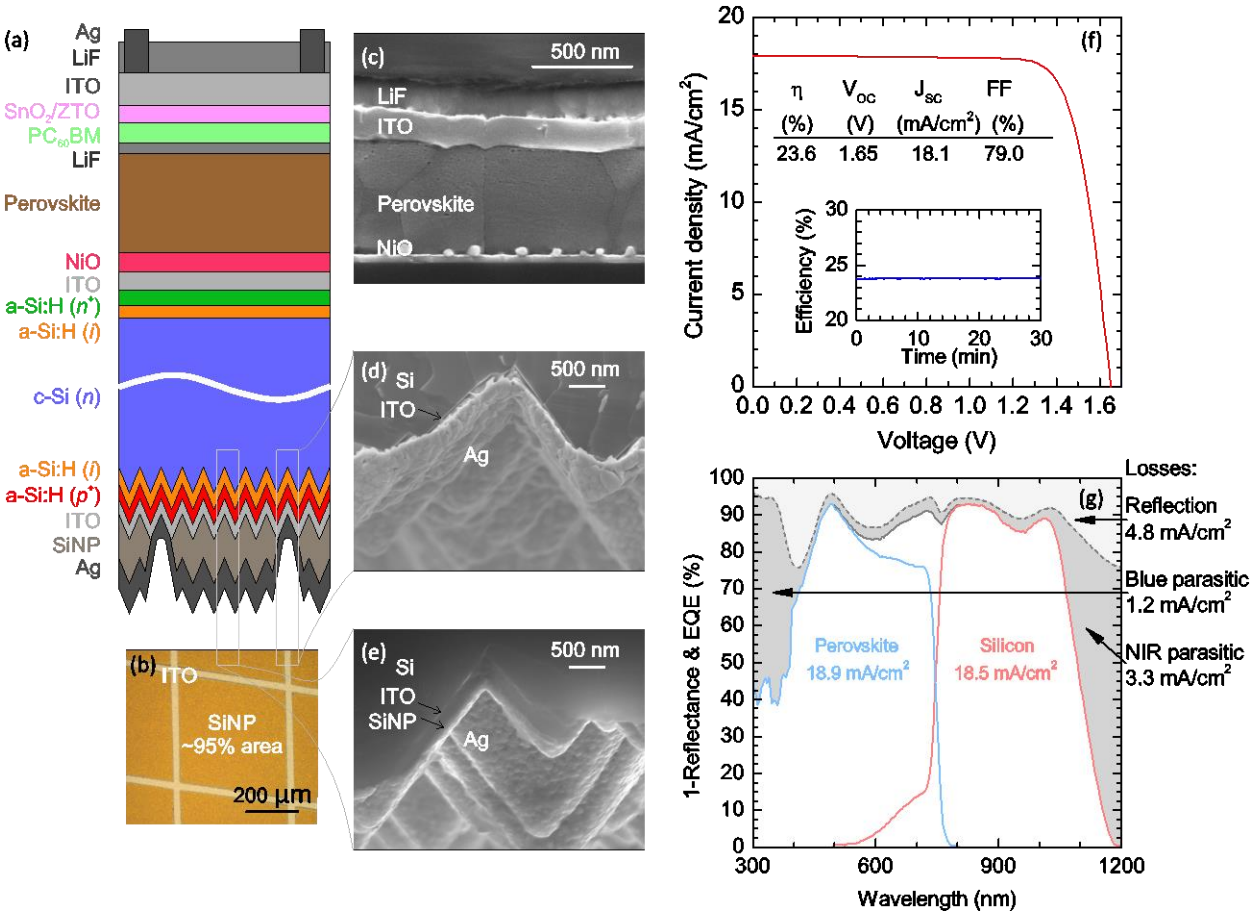

Figure 2. Design and performance of the perovskite/silicon tandem cell. (a) Schematic of the perovskite/silicon tandem solar cell (not to scale), (b) optical microscope image of the silicon-nanoparticle-patterned rear side of the silicon cell before silvering, (c) cross-sectional SEM image of the perovskite top cell, (d) cross-sectional SEM image of the rear side of the silicon cell in an area with no silicon nanoparticles, (e) cross-sectional SEM image of the rear side of the silicon cell in an area with silicon nanoparticles, (f) J-V curve (NREL certified, see Supplementary Figure 8) and efficiency at the maximum power point (inset) of the champion tandem device, (g) total absorbance (1-R, where R is the reflectance; dashed grey line), EQE of the perovskite top cell (solid blue line), and EQE of the silicon bottom cell (solid red line). The sum of the EQEs is denoted by the solid grey line. The light and dark grey shaded areas represent the light lost to reflection and parasitic absorption, respectively, and the associated current density losses are indicated.

To form two-terminal perovskite/silicon tandem solar cells, perovskite cells were fabricated directly on top of complete silicon bottom cells, as shown in Figure 2a. The perovskite top cells, one of which is shown in cross section in Figure 2c, were identical to their single-junction predecessors, except we annealed the NiO_x layer at 190 °C for 10 hours instead of 300 °C for 1 hour to prevent appreciable deterioration of the surface passivation layers in the underlying silicon cell. We chose an amorphous silicon / crystalline silicon heterojunction solar cell design for the bottom cell because of its high

V_{OC}, which results from the separation of the highly recombination-active (ohmic) contacts from the silicon absorber bulk, and because its dominant performance-loss mechanism under the standard solar spectrum—parasitic absorption of blue light in the front amorphous silicon (a-Si:H) layers—is irrelevant in tandems.

The silicon cell fabrication process was adjusted to tune the silicon cells to the infrared spectrum that they receive in the tandem, as well as for compatibility with the spin-coated perovskite top cells. In particular, the a-Si:H layers on both sides were slightly thickened to enhance passivation and carrier collection (the resulting visible parasitic absorption is not detrimental in tandems)[45]. A wafer with a chemical-mechanical polished front surface was used to allow for top-cell spin coating, but the rear of wafer was textured to form random pyramids. The pyramids scatter weakly absorbed near-bandgap light, elongating its path length through the wafer and enhancing the cell's infrared EQE. An excellent rear reflector comprising a silicon nanoparticle (SiNP) / silver stack was also implemented. The SiNP layer, which is atypical in silicon heterojunction solar cells, is used because of its low refractive index—with a porosity of approximately 60%, its refractive index is 1.4—and high transparency at wavelengths longer than 1000 nm. More details on the use and fabrication of the rear reflector comprising a SiNP / silver stack will be presented in a subsequent publication. Inserting a thick, low-refractive-index layer between the wafer and metal reflector increases the rear internal reflectance by reducing the fraction of light that reaches the lossy metal layer[46], and a SiNP / silver reflector has a rear internal reflectance of over 99%[47]. Finally, the front ITO layer was thinned to reduce infrared parasitic absorption since it does not need to play the role of antireflection coating in tandems and because, unlike in a single-junction silicon cell, the lateral conductivity of the front electrode need not be high.

In more detail, following the fabrication sequence, an *n*-type, 280-µm-thick, double-side polished, float-zone (FZ) silicon wafer was textured only on its rear side in an alkaline solution, resulting in the formation of random pyramids. Intrinsic and *p*-type a-Si:H films (7 and 15 nm thick, respectively) were first deposited by plasma-enhanced chemical vapor deposition on the textured (rear) side of the wafer, and intrinsic and *n*-type a-Si:H films (7 and 8 nm thick, respectively) were then deposited on the polished (front) side. A 20-nm-thick, highly transparent ITO layer was next sputtered on the front side through a shadow mask, defining 11 mm x 11 mm square cells, to act as a recombination junction between the silicon and perovskite cells. A 20-nm-thick, highly transparent ITO layer was also deposited over the rear side through the same shadow mask, followed by a 300-nm-thick SiNP layer spray coated through a stainless-steel mesh to define local openings[48], and finally, a 200-nm-thick silver layer. Figure 2b shows a plan-view microscope image of the patterned SiNP layer before silver sputtering; the 5% uncoated area allows the silver to make direct electrical contact to the underlying ITO layer (Figure 2d), whereas the SiNPs in the remaining area (Figure 2e) enhance infrared conversion efficiency.

On its own, the silicon bottom cell has an efficiency well below 10% because of low *FF* caused by the high sheet resistance of the thin front ITO layer and lack of metal fingers, and because of low short-circuit current density (J_{SC}) caused by the high reflectance of the planar front surface and lack of appropriate anti-reflection coating. The best 4 cm^2 silicon heterojunction solar cell fabricated by the same lab with the same—but double-side-textured—wafers, adjusted deposition processes, and screen-printed silver

fingers reached an NREL-certified efficiency of 21.4%. A comparable 1 cm^2 cell (as in the tandem) is expected to have an efficiency approximately 0.3% lower because of a 10 mV V_{OC} loss from increased edge recombination, and a comparable cell with a planar front surface (as in the tandem) is expected to reach only 19–20%.

Figure 2f displays the *J-V* characteristic of the champion tandem cell, certified at NREL, with a V_{OC} of 1.65 V, J_{SC} of 18.1 mA/cm^2, and *FF* of 79.0%, resulting in an efficiency of 23.6% with a 1 cm^2 aperture area and no hysteresis, as shown in Supplementary Figure 9. The tandem was held at its maximum power point for over half an hour, under constant illumination, and maintained 23.6% efficiency. Supplementary Figure 11 shows performance metrics for our final batch of devices without IR reflector: V_{oc} = 1.64 ±0.02V, J_{sc} = 17.5 ±0.2 mAcm^{-2}, FF = 79.9 ±1.0 %, and η = 22.8 ±0.4 % and with IR reflectors V_{oc} = 1.64 ±0.01V, J_{sc} = 18.2 ±0.2 mAcm^{-2}, FF = 78.1 ±1.0 %, and η = 23.3 ±0.4 %. The high performance and narrow statistical distribution for these 1 cm^2 cells—which are large-area amongst present perovskite devices—attests to the ability of the pulsed-CVD process to deposit a window layer that prevents pinholes and shunt pathways.

Figure 2g shows the measured total absorbance (1-reflectance) and EQE of both sub-cells in the perovskite/silicon tandem solar cell. The figure has been divided into several (colored) regions to help visualize the tandem response and loss mechanisms. Integrating the EQE spectra over the AM 1.5G spectrum reveals that the perovskite top cell and silicon bottom cell generate 18.9 mA/cm^2 and 18.5 mA/cm^2, respectively. We note that the silicon cell EQE exceeds 90% between 800 and 875 nm, which is much higher than the measured transmittance of the single-junction perovskite cell in Figure 1c. This high EQE results from a thinner ITO electrode (20 nm between the silicon and perovskite in the tandem instead of 170 nm between the perovskite and glass in the single-junction cell) and reduced reflection due to the lack of an air interface in the tandem. Supplementary Figures 9 and 11 illustrate the efficacy of the SiNP rear reflector in increasing infrared absorption within the silicon wafer, corresponding to an increase in J_{SC} of about 1.5 mA/cm^2. Two main current losses are front-surface reflection (area above the total absorbance curve) and parasitic absorption (area between the total absorbance and EQE curves), which account for 4.8 mA/cm^2 and 4.5 mA/cm^2, respectively. To further improve the J_{SC} of the tandem device, the easiest step would be to reduce front-surface reflection. Were it eliminated, the summed J_{SC} would increase by 4.2 mA/cm^2. As parasitic absorption still exists, not all transmitted photons would be converted into electron-hole pairs. The short-wavelength parasitic absorption loss associated with the first pass through the layers at the front of the solar cell is 1.2 mA/cm^2—0.7 mA/cm^2 from the ITO and 0.5 mA/cm^2 from the PCBM and SnO_2/ZTO bilayer, according to our optical simulations—and all of this would be gained as current in the top cell if the parasitic absorption were eliminated. The infrared parasitic absorption, which may occur in any layer in the tandem, appears to be large at 3.3 mA/cm^2, but this “loss” is misleading because not all of this current is available to be gained. Eliminating infrared parasitic absorption will result in a J_{SC} gain (in the bottom cell) of less than half that value because—even assuming Lambertian light trapping—much of the light will escape out the front of the cell and contribute to the measured reflectance.

Improved Stability of Perovskite Solar Cells

Early in the project we showed that[38], in addition to acting as a highly transparent and conductive electrode, ITO—by virtue of its behavior as a diffusion barrier—can significantly increase the thermal and environmental stability of a perovskite solar cell by essentially trapping the volatile methylammonium cation[49]. The increased thermal stability of the thermodynamically favorable[27] mixed CsFA perovskite compared to the pure methylammonium perovskite[26], along with the dense, pinhole-free ALD SnO_2/ZTO bilayer, should result in perovskite solar cells with even greater stability than previously reported. We tested the stability of single-junction CsFA mixed perovskite solar cells by operating 0.48 cm^2-aperture-area devices at the maximum power point without additional encapsulation under continuous, one-sun-equivalent, visible illumination with a sulfur plasma lamp. The test was performed in ambient conditions with an average room humidity of around 40% and the lamp heating the samples to 35 °C. Remarkably, the devices operated with minimal degradation in performance for over 1000 hours of testing, as shown in Figure 3a. In our previous study, small dust particles in the perovskite resulted in pinholes in the ITO encapsulation, creating a pathway for methylammonium evolution and causing eventual efficiency degradation[38]. In the present CsFA devices, however, no such pinhole-based degradation was apparent after 1000 hours of operation, speaking to the efficacy of the conformal ALD process to prevent pinhole formation and to the overall increased stability of the CsFA perovskite.

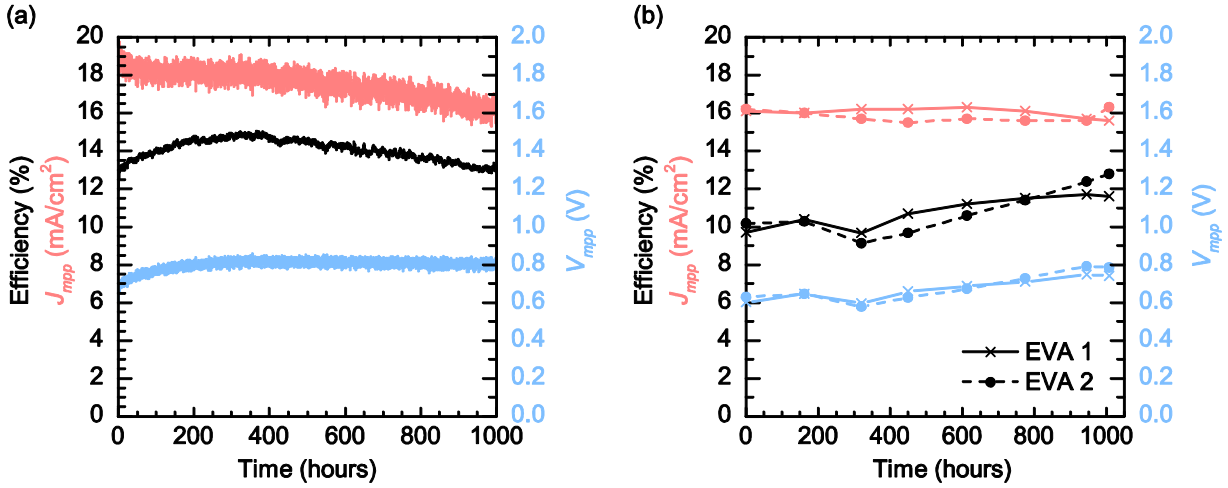

Figure 3. Stability of perovskite top cell. (a) Efficiency (black), J_{MPP} (red), and V_{MPP} (blue) of a single-junction perovskite device with no additional encapsulation during 1000 hours of continuous maximum-power-point tracking, (b) efficiency (black), J_{MPP} (red), and V_{MPP} (blue) of a single-junction perovskite device packaged with EVA, glass, and a butyl rubber edge seal during damp-heat testing.

Although the cell in Figure 3a had the same efficiency after 1000 hours as at the start of the test, this efficiency was not constant over the testing period. As can be seen in Figure 3a, the rise in efficiency during the first 400 hours corresponds to an increase in voltage (V_{MPP}), likely indicating the improvement of the NiO/perovskite interface or increased perovskite crystallinity. V_{MPP} started at only a modest value but the lack of V_{MPP} decay during the test is noteworthy. Falling current density (J_{MPP}) is the culprit for the decrease in efficiency over the last 600 hours of the test. The exact cause of this decrease in J_{MPP} is presently being studied, but potential causes are the lack of an edge seal or

pinholes in the ITO layer caused by dust particles; either case would lead to evolution of the organic cation. However, both of these potential issues can be solved through proper device encapsulation. The vast majority of commercial silicon solar modules are encapsulated with the elastomeric polymer ethylene-vinyl acetate (EVA) and a glass cover sheet to prevent oxidation and moisture ingress, and thus to enable >25-year lifetimes. Lamination of EVA is typically performed at 110–150 °C for 30 min under mild vacuum. The increased thermal stability[38] of our perovskite devices with the sputtered ITO electrode enables us to compare the stability of our devices directly to conventional silicon modules by packaging our devices using this industry-standard encapsulation process. We laminated single-junction perovskite devices between two sheets of glass with EVA at a curing temperature of 140 °C for 20 minutes. A butyl rubber edge seal was used to prevent moisture ingress.

In order to test the efficacy of this packaging, we performed the damp heat test described in the International Electrotechnical Commission (IEC) design qualification testing protocol 61215 for “Crystalline Silicon Terrestrial Photovoltaic (PV) Modules.” These are accelerated lifetime tests with the goal of rigorously testing modules for the same failure mechanisms observed in the field in a much shorter time. The damp-heat test requires that the module operate at 85 °C and 85% relative humidity for 1000 hours with no more than 10% degradation in performance. We performed this damp heat test on two packaged perovskite devices over the course of 6 weeks (1008 hours). The devices were taken out of the dark damp heat chamber once a week and measured with a maximum-power-tracking program until the efficiency stabilized. Figure 3b shows the voltage, current, and efficiency at maximum power each week. Not only do the devices pass the damp heat test, they improve over the course of the test. While the efficiency of the devices is initially limited by poor *FF*, V_{MPP} increases throughout the test, similar to under continuous illumination (Figure 3a). However, unlike in the continuous-illumination study, J_{MPP} remains constant throughout the course of the damp-heat test, indicating that the packaging successfully addressed potential problems such as pinholes in the ITO and an improper edge seal.

In the last year of the project after the publication of the *Nature Energy* paper, we made the following improvements that should enable our next generation tandem to have 25-27 % efficiency.

- Replace ITO with IZO (Indium zinc oxide) to reduce near infrared (IR) absorption so that the Si cell will generate more current.
- Make the transparent conducting oxide (TCO) layer thinner to reduce parasitic absorption and maintain the sheet resistance by using metal gridlines
- Use PDMS scattering layer on top of the tandem to improve light trapping.

- Increase the band gap of the perovskite from 1.63 eV to 1.68 eV, which is the optimal value for tandems on silicon taking into account imperfect absorption at the band edge of the perovskite.
- Improve the voltage of perovskite cell from 0.9 V to 1.1 V by using PTAA as the selective hole contact instead of NiO.
- Improve the fill factor by having the selective contacts be thin and as conductive as we can make them without introducing parasitic absorption.

Unfortunately, we have not been able to implement all of these improvements during the same week to reap all of the benefits at the same time. On many occasions we have made perovskite solar cells that were more efficient than we had ever made before on glass, but were then not able to get the performance we expected when we made the device on top of a silicon solar cell. We have learned several important lessons. First, when we use extremely thin selective contacts for the purpose of minimizing parasitic absorption, our cells can easily be shorted if the layers have pinholes. Second, whenever we change a layer in the device stack, there can be consequences for every subsequent layer that is deposited. For example, we have learned that our ALD process for depositing tin oxide on top of the perovskite has to be modified when we change layers below the perovskite layer. Third, it is challenging to make a high-performance device in four different labs using multi-user tools that are used for many other projects. Sometimes the tools are contaminated and at other times they are broken. Consequently, we only occasionally have windows of opportunity to make world record tandems. Going forward over the next several years it will be helpful to acquire dedicated tools for more of the processing steps.

References for Section 1

1. NREL Efficiency Table Rev. 08-08-2016. (2016). at <http://www.nrel.gov/ncpv/images/efficiency_chart.jpg>

2. Wolf, S. De *et al.* Organometallic Halide Perovskites : Sharp Optical Absorption Edge and its Relation to Photovoltaic Performance. *J. Phys. Chem. Lett.* **5,** 1035–1039 (2014).

3. Stranks, S. D. *et al.* Electron-Hole Diffusion Lengths Exceeding. *Science* **342,** 341–344 (2014).

4. Brandt, R. E., Stevanović, V., Ginley, D. S. & Buonassisi, T. Identifying defect-tolerant semiconductors with high minority carrier lifetimes: Beyond hybrid lead halide perovskites. *MRS Commun.* **5,** 265–275 (2015).

5. Noh, J. H., Im, S. H., Heo, J. H., Mandal, T. N. & Seok, S. Il. Chemical management for colorful, efficient, and stable inorganic-organic hybrid nanostructured solar cells. *Nano Lett.* **13,** 1764–1769 (2013).

6. Bailie, C. D. *et al.* Semi-transparent perovskite solar cells for tandems with silicon and CIGS. *Energy Environ. Sci.* **8,** 956–963 (2014).

7. Todorov, T., Gershon, T., Gunawan, O., Sturdevant, C. & Guha, S. Perovskite-kesterite monolithic tandem solar cells with high open-circuit voltage. *Appl. Phys. Lett.* **105,** 173902 (2014).

8. Mailoa, J. P. *et al.* A 2-terminal perovskite/silicon multijunction solar cell enabled by a silicon tunnel junction. *Appl. Phys. Lett.* **106,** 121105 (2015).

9. Löper, P. *et al.* Organic–inorganic halide perovskite/crystalline silicon four-terminal tandem solar cells. *Phys. Chem. Chem. Phys.* **17,** 1619–1629 (2015).

10. Albrecht, S. *et al.* Monolithic perovskite/silicon-heterojunction tandem solar cells processed at low temperature. *Energy Environ. Sci.* **9,** 81–88 (2016).

11. Werner, J. *et al.* Sputtered rear electrode with broadband transparency for perovskite solar cells. *Sol. Energy Mater. Sol. Cells* **141,** 407–413 (2015).

12. Kranz, L. *et al.* High-Efficiency Polycrystalline Thin Film Tandem Solar Cells. *J. Phys. Chem. Lett.* **6,** 2676–2681 (2015).

13. Yang, Y. M. *et al.* Multilayer Transparent Top Electrode for Solution Processed Perovskite/Cu(In,Ga)(Se,S)2 Four Terminal Tandem Solar Cells. *ACS Nano* **9,** 7714–21 (2015).

14. Chen, B. *et al.* Efficient Semitransparent Perovskite Solar Cells for 23.0%-Efficiency Perovskite/Silicon Four-Terminal Tandem Cells. *Adv. Energy Mater.* **6,** 1–7 (2016).

15. Werner, J. *et al.* Efficient Monolithic Perovskite/Silicon Tandem Solar Cell with Cell Area >1 cm2. *J. Phys. Chem. Lett.* **7,** 161–166 (2016).

16. Yang, Z. *et al.* Stable Low-Bandgap Pb-Sn Binary Perovskites for Tandem Solar Cells. *Adv. Mater.* **28,** 8990–8997 (2016).

17. Fu, F. *et al.* Low-temperature-processed efficient semi-transparent planar perovskite solar cells for bifacial and tandem applications. *Nat. Commun.* **6,** 8932 (2015).

18. Eperon, G. E. *et al.* Perovskite-perovskite tandem photovoltaics with ideal bandgaps. *Science.* **9717,** 1–9 (2016).

19. Lal, N. N., White, T. P. & Catchpole, K. R. Optics and light trapping for tandem solar cells on silicon. *IEEE J. Photovoltaics* **4,** 1380–1386 (2014).

20. Bailie, C. D. & McGehee, M. D. High-efficiency tandem perovskite solar cells. *MRS Bull.* **40,** 681–686 (2015).

21. Ginley, D. S., Hosono, H. & Paine, D. C. *Handbook of transparent conductors*. *Handbook of Transparent Conductors* (2011). doi:10.1007/978-1-4419-1638-9

22. Liao, L. S. *et al.* Ion-beam-induced surface damages on tris-(8-hydroxyquinoline) aluminum. *Appl. Phys. Lett.* **75,** 1619 (1999).

23. Leijtens, T. *et al.* Stability of Metal Halide Perovskite Solar Cells. *Adv. Energy Mater.* **5,** 1–23 (2015).

24. Liu, P. *et al.* Interfacial electronic structure at the CH3NH3PbI3 / MoOx interface. *Appl. Phys. Lett.* **106,** 193903 (2015).

25. Yang, W. S. *et al.* High-performance photovoltaic perovskite layers fabricated through intramolecular. *Science.* **348,** 1234–1237 (2015).

26. Lee, J. W. *et al.* Formamidinium and cesium hybridization for photo- and moisture-stable perovskite solar cell. *Adv. Energy Mater.* **5,** 1–9 (2015).

27. Yi, C. *et al.* Entropic stabilization of mixed A-cation ABX 3 metal halide perovskites for high performance perovskite solar cells. *Energy Environ. Sci.* **9,** 656–662 (2016).

28. Liu, X. *et al.* Spray Reaction Prepared FA1-xCsxPbI3 Solid Solution as Light Harvester for Perovskite Solar Cells with Improved Humidity Stability. *RSC Adv.* **6,** 14792–14798 (2016).

29. McMeekin, D. P. *et al.* A mixed-cation lead mixed-halide perovskite absorber for tandem solar cells. *Science.* **351,** 151–155 (2016).

30. Saliba, M. *et al.* Cesium-containing triple cation perovskite solar cells: improved stability, reproducibility and high efficiency. *Energy Environ. Sci.* **9,** 1989–1997 (2016).

31. Bakke, J. R., Pickrahn, K. L., Brennan, T. P. & Bent, S. F. Nanoengineering and interfacial engineering of photovoltaics by atomic layer deposition. *Nanoscale* **3,** 3482–3508 (2011).

32. Palmstrom, A. F., Santra, P. K. & Bent, S. F. Atomic layer deposition in nanostructured photovoltaics: tuning optical, electronic and surface properties. *Nanoscale* **7,** 12266–12283 (2015).

33. Kim, B.-J. *et al.* Highly efficient and bending durable perovskite solar cells: toward wearable power source. *Energy Environ. Sci.* **8,** 916–921 (2015).

34. Baena, J. P. C. *et al.* Highly efficient planar perovskite solar cells through band alignment engineering. *Energy Environ. Sci.* **8,** 2928–2934 (2015).

35. Zhu, Z. *et al.* Enhanced Efficiency and Stability of Inverted Perovskite Solar Cells Using Highly Crystalline SnO2 Nanocrystals as the Robust Electron-Transporting Layer. *Adv. Mater.* **28,** 6478–6484 (2016).

36. You, J. *et al.* Improved air stability of perovskite solar cells via solution-processed metal oxide transport layers. *Nat. Nanotechnol.* **11,** 1–8 (2015).

37. Kim, J. H. *et al.* High-Performance and Environmentally Stable Planar Heterojunction Perovskite Solar Cells Based on a Solution-Processed Copper-Doped Nickel Oxide Hole-Transporting Layer. *Adv. Mater.* **27,** 695–701 (2015).

38. Bush, K. A. *et al.* Thermal and Environmental Stability of Semi-Transparent Perovskite Solar Cells for Tandems Enabled by a Solution-Processed Nanoparticle Buffer Layer and Sputtered ITO Electrode. *Adv. Mater.* **28,** 3937–3943 (2016).

39. Mullings, M. N., Hägglund, C. & Bent, S. F. Tin oxide atomic layer deposition from tetrakis(dimethylamino)tin and water. *J. Vac. Sci. Technol. A Vacuum, Surfaces, Film.* **31,** 61503 (2013).

40. Guziewicz, E. *et al.* ALD grown zinc oxide with controllable electrical properties. *Semicond. Sci. Technol.* **27,** 74011 (2012).

41. Despeisse, M. *et al.* Resistive interlayer for improved performance of thin film silicon solar cells on highly textured substrate. *Appl. Phys. Lett.* **96,** 10–13 (2010).

42. Larson, B. W. *et al.* Thermal [6,6] -> [6,6] Isomerization and Decomposition of PCBM (Phenyl-C61-butyric Acid Methyl Ester). *Chem. Mater.* **26,** 2361–2367 (2014).

43. Mullings, M. N. *et al.* Thin film characterization of zinc tin oxide deposited by thermal atomic layer deposition. *Thin Solid Films* **556,** 186–194 (2014).

44. Hägglund, C. *et al.* Growth, intermixing, and surface phase formation for zinc tin oxide nanolaminates produced by atomic layer deposition. *J. Vac. Sci. Technol. A Vacuum, Surfaces, Film.* **34,** 21516 (2016).

45. Holman, Z. C. *et al.* Current Losses at the Front of Silicon Heterojunction Solar Cells. *IEEE J. Photovoltaics* **2,** 7–15 (2012).

46. Holman, Z. C. *et al.* Infrared light management in high-efficiency silicon heterojunction and rear-passivated solar cells. *J. Appl. Phys.* **113,** 13107 (2013).

47. Holman, Z. C., De Wolf, S. & Ballif, C. Improving metal reflectors by suppressing surface plasmon polaritons: a priori calculation of the internal reflectance of a solar cell. *Light Sci. Appl.* **2,** 1–6 (2013).

48. Holman, Z. C. & Kortshagen, U. R. A flexible method for depositing dense nanocrystal thin films: impaction of germanium nanocrystals. *Nanotechnology* **21,** 335302 (2010).

49. Kim, I. S. & Martinson, A. B. F. Stabilizing hybrid perovskites against moisture and temperature via non-hydrolytic atomic layer deposited overlayers. *J. Mater. Chem. A* **3,** 20092–20096 (2015).

Project Results from MIT:

Within the course of this project, perovskite on silicon tandem solar cells have demonstrated the ability to reach high efficiencies. An efficiency of more than 25% was demonstrated at EPFL for a four-terminal setup[1], and we demonstrated 23.6% efficiency in an integrated two-terminal setup. Perovskite on silicon tandem solar cells are now approaching the efficiencies of the best single-junction silicon solar cells, surpassing which is a requirement for their commercial success.

High efficiency, however, is not the only requirement for an economically successful tandem. In a study published in RSC Advances[2], we have shown that for a tandem solar cell to be economically successful, it should be a “marriage of equals”. This marriage of equals implies that the sub-cells should have similar single-junction efficiencies, similar fabrication costs and similar integration costs. Current efficiency records are achieved using costly silicon-technologies, like *n*-type silicon heterojunction solar cells, which serve well to establish efficiency potentials, but aren’t good matches in

[1] J. Werner et al., *ACS Energy Lett.*, 2016, 1 (2), pp 474–480
[2] M. Peters, S. Sofia, T. Buonassisi, *RSC Advances* 6 (2016), 66911 – 66923.

terms of fabrication cost. Moreover, in a different study, the MIT group has shown that reducing the capital intensity (CAPEX) in solar cell technology is essential to reach climate goals[3]. These findings motivated us to concentrate on bottom cell technologies with a low-cost, low-capex signature. An examples for such a technology is *p*-type multicrystalline silicon, the working horse of today's manufacturing.

The goal of our approach was to transfer methods and technologies established within this project onto these new materials. One step here included transferring the top-cell structure, originally developed for *n*-type silicon material, to *p*-type. This step required developing a different tunnel junction. The transfer to p-type enables not only enables access to the vast majority of silicon solar cells currently in production, but also to upcoming technologies with low-cost potential, like kerfless silicon. Additionally, we wanted to establish which properties of the standard *p*-type solar cell design are most and least important when this cell is operated as a bottom cell in a tandem, rather than in single junction configuration. For this purpose, we developed a loss-analysis method for the tandem solar cell.

P-type silicon bottom cell fabrication

To allow the deposition of the top perovskite subcell and fabricate a cost-effective, high efficiency two-terminal tandem, the following device requirements for the *p*-type Si bottom subcell were defined: mirror like front polished surface, high single junction efficiency (comparable to commercial single junction Si cells), no oxide layers and highly uniform front surface, low production cost and capital expenditure. In this context, two low-capex *p*-type bottom Si architectures that could satisfy these requirements were fabricated and measured: BSF (back surface field) and LBSF (local-area back surface field) solar cells. Due to its higher efficiency and little additional cost compared to the BSF architecture, the LBSF cell was chosen as a suitable cell for a perovskite-Si device.

A batch of LBSF bottom Si subcells was fabricated with a single junction reference efficiency of 16.8% under AM 1.5G spectrum. These cells were adapted for bottom subcell operation by 1) using a polished front surface wafer, 2) optimizing the firing and back contact deposition, 3) establishing adequate cleaning and oxide etching procedures before tunnel junction deposition, 4) defining an effective and easy-to-remove masking stack to protect the cells in intermediate steps and reducing the voltage loss in the ITO/Si interlayer.

Figure 3 shows the pseudo I-V curves of the bottom cell after different steps of tunneling layer deposition measured by Suns-Voc.

[3] D. Berney Needleman et al., Energy & Environmental Science 9 (6), 2122-2129

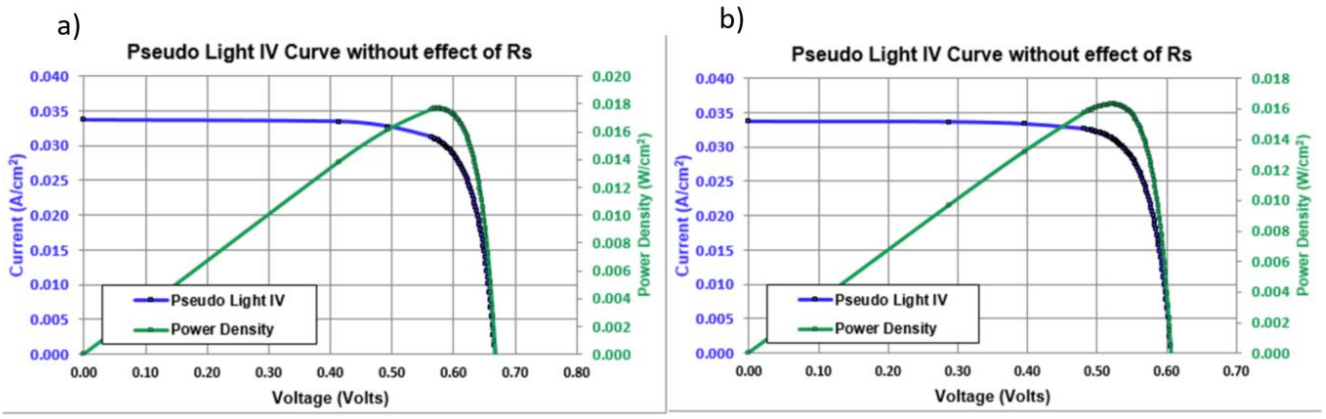

Figure 3: Pseudo J-V curves for bottom Si cells, after a) ITO deposition, b) NiOx deposition.

Tandem on *p*-type silicon bottom cell

World records for silicon single-junction or silicon based tandem solar cells are achieved with *n*-type base material. It is generally agreed that *n*-type material has the higher efficiency potential, however processing of *n*-type high efficiency architectures is more costly than processing architectures using the current industry standard base material, which is *p*-type. Switching from *n*-type to *p*-type requires inverting the perovskite solar cell and, hence, changing the recombination contact. The main enabling step here was that we established an ITO/NiOx double layer as recombination contact. We could demonstrate that the voltage of the sub cells is adding up, which proves the functionality of the recombination contact.

Figure 4summarizes our results achieved for a $1cm^2$ monolithic tandems, using ITO/NiOx recombination contacts and measured under 1 sun AM 1.5_G illumination. Figure 4 (a) shows the device structure of two tandems with Al-BSF and PERC-passivated p-type silicon bottom cells. In figure 4 (b) the band structure of the ITO/NiOx recombination contact on a *p*-type silicon cell is sketched out. Figure 4 (c) is a cross-sectional scanning electron microscopy image of a tandem solar cell with a PERC-type silicon bottom cell. The cross-section is similar to the tandem on the Al-BSF cell. Exceptions are that the Al-BSF cell was rear-textured and did not have the thin passivation layers. The current-voltage characteristics swept at 100 mVs^{-1} in both forward (solid line) and reverse (dashed line) direction are shown in figure 4 (d) for the tandem with an Al-BSF bottom cell. The stabilized short-circuit current density, maximum power point, and open-circuit voltage are shown as black diamonds. The current-voltage characteristics for a semitransparent $Cs_{0.17}FA_{0.83}Pb(Br_{0.17}I_{0.83})_3$ perovskite solar cell and unfiltered silicon single-junction device made from the same p-type silicon wafer as the bottom cell are also shown. Figure 4(e) shows power density and current density vs. time measured at the maximum power point. The inset is the open-circuit voltage vs. time over a period of 30 min. 1-*R* (reflectance) of the tandem and external quantum efficiency of the top and bottom cells for tandems with are depicted in figure 4 (f) for the Al-BSF- and in (g) for the PERC-passivated bottom cell. We note that the EQE of the PERC bottom cell was calculated by multiplying the IQE of the unfiltered silicon cell with the transmittance of the semitransparent perovskite top cell.

This gave a lower estimate of the bottom cell EQE (blue). The upper estimate (gray) was obtained by accounting for the effects of the transmittance and reflectance of the ITO/glass substrate on the transmittance of the top cell. Figure 4 (h) shows the current-voltage characteristics of the tandem using a PERC-type bottom cell, and (i) shows the power density and current density at the maximum power over 288 min under 1 sun illumination.

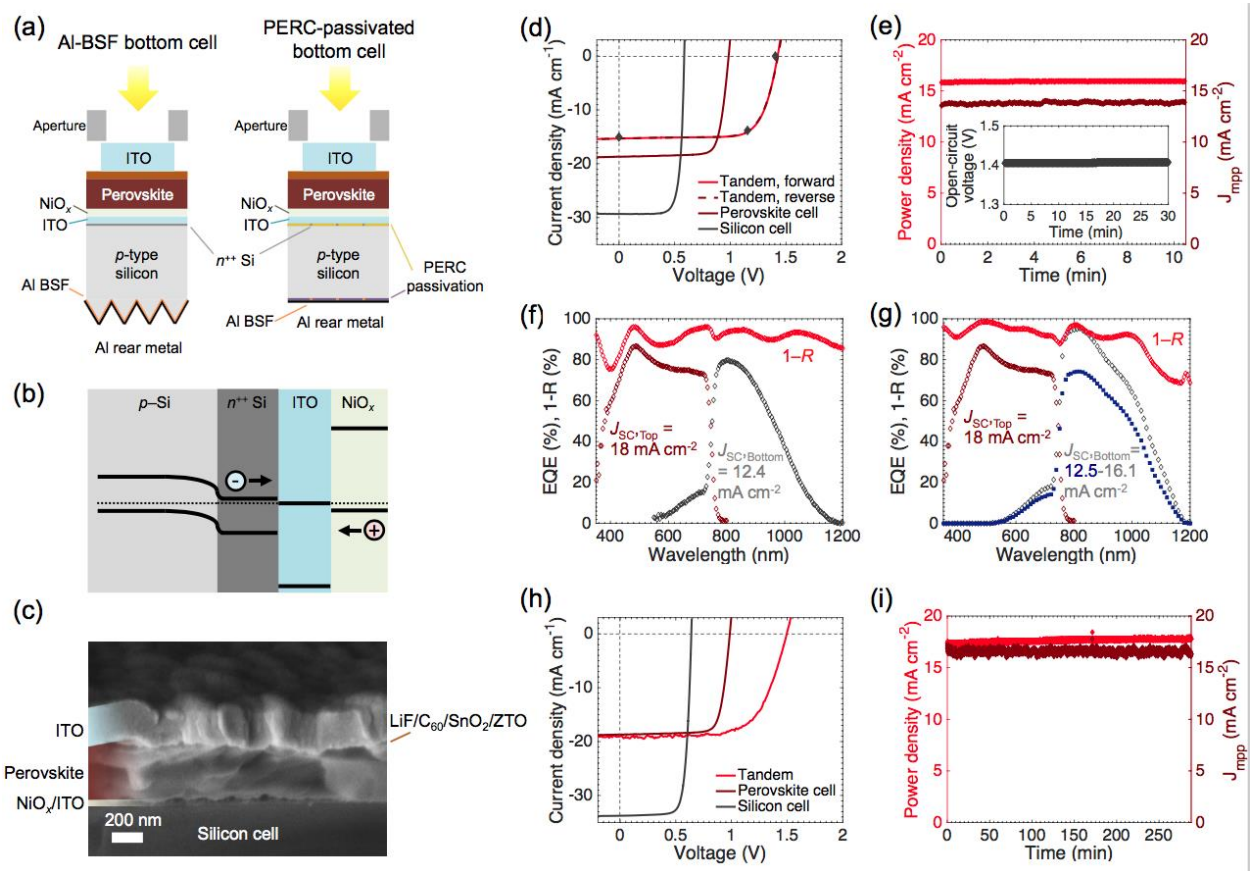

Figure 4: (a) Device structure of two tandems. (b) Band structure of the ITO/NiOx recombination contact on a p-type silicon cell. (c) Cross-sectional SEM image of tandem with PERC-type bottom cell. (d) J–V curves in forward (solid line) and reverse (dashed line) direction. (e) Power density and current density vs. time measured at the maximum power point. The inset shows open-circuit voltage vs. time over a period of 30 min. (f) 1-R (reflectance) of the tandem and external quantum efficiency of the top and bottom cells for the Al-BSF bottom cell (g) PERC-type bottom cells. Tandem with PERC-passivated cell: (h) J–V curve of the tandem, bottom cell and top cell, and (i) maximum power point power density and current density over 288 min under 1 sun.

Remaining challenges with this architecture include increasing current density and efficiency. Transferring the developed structure onto a *p*-type bottom cell has proved more challenging than anticipated. The highest stable efficiency so far achieved is 17.8%. This marks a considerable improvement over initial efficiencies (14%), but is lower than what we had expected (19-20%). Challenges include achieving high currents in the bottom cell and reproducing the very high voltages achieved with either sub cell

separately. These issues can, in part, be attributed to non-uniformities in the cell and can be addressed by introducing evaporation for some of the deposition steps.

Voltage loss analysis for the bottom cell

Based on the established methodology for finding an open-circuit voltage breakdown in LBSF devices in literature, we developed a voltage loss analysis methodology to characterize the bottom Si subcell and the tunnel junction. The methodology is based in contactless Quasi-steady state photoconductance (QSS-PC) and photoluminescence (PL) measurements of semi-fabricated structures. The voltage of the structures without metallization is measured by QSS-PC, and used for a self-consistent calibration procedure of the metalized samples. In contrast with other voltage loss analysis methodologies, this experimental setup allows to obtain the voltage loss of various critical processing steps with high detail without the need of complex computational models. The different test structures are shown in Figure 5.

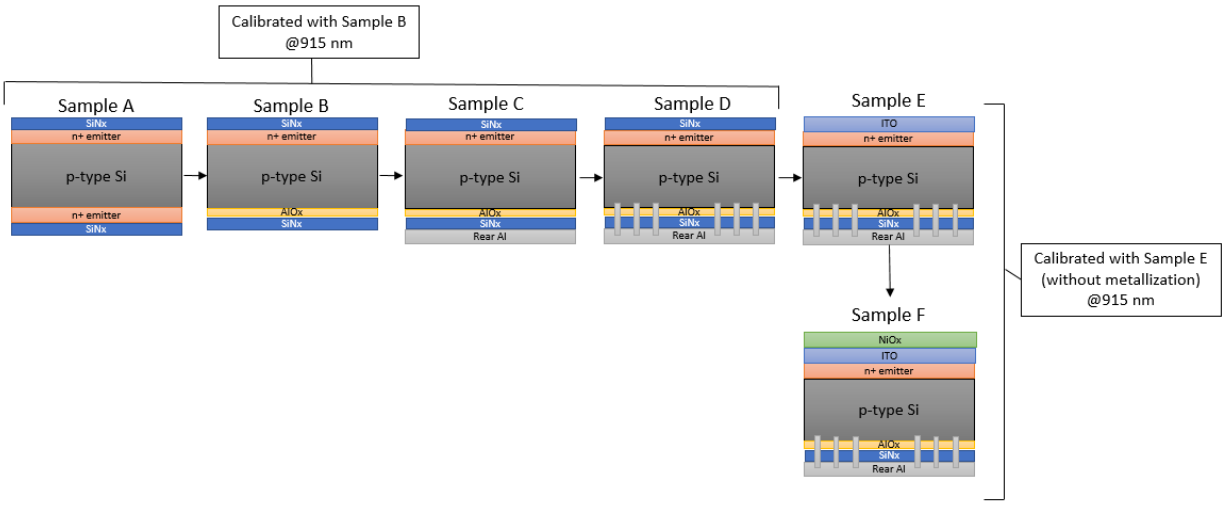

Figure 5: Final voltage loss breakdown after a-Si layer deposition.

Applied to LBSF bottom Si subcell, the voltage loss analysis provides a loss breakdown of the main voltage loss mechanics as a function of the V_{OC} and the recombination current Jo of the device. The ITO deposition step was identified as producing the greatest voltage loss, with a Jo contribution of 264.67 fA/cm^2. This loss was likely caused by the sputtering procedure affecting the Si front surface, and the scarce surface passivation provided by the ITO layer. To reduce this loss, an a-Si stack was deposited between the Si surface and the ITO layer to reduce the recombination losses. The a-Si stack was found to reduce the voltage losses significantly, and the new measured Jo was 44.64 fA/cm^2. The results for the entire stack are shown in Figure 6.

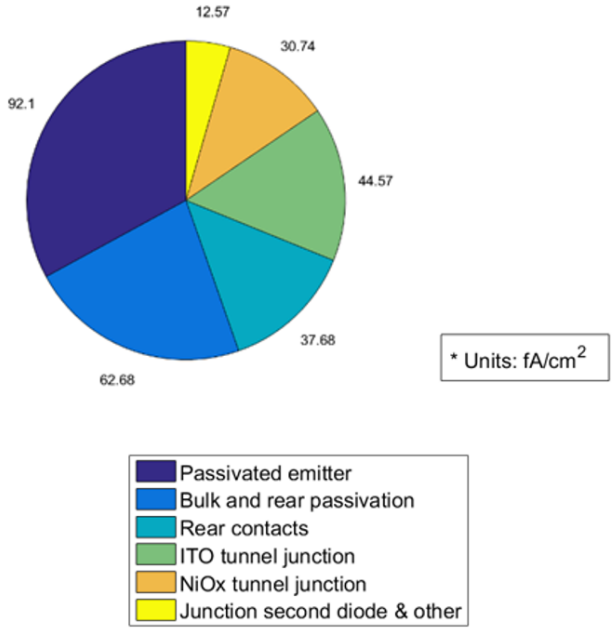

Figure 6: Semi-fabricated samples used for the voltage loss analysis procedure.

We suggest various pathways for expanding the analysis to the top perovskite subcell. The main challenge for performing calibrated PL measurement of perovskite devices is the difficulty of measuring the excess carrier density or V_{OC} of intermediate structures in the 2T tandem device. In this scenario, several option were suggested: 1) probing a 3T multijunction device to find the V_{OC} of the top perovskite subcell for various illumination intensities, 2) exciting the perovskite junction and measuring the V_{OC} of the whole tandem, subtracting any parasitic PL emission. Furthermore, future work should focus in finding suitable interlayers between ITO, or other similar tunneling layer such as IZO, and the Si emitter. The voltage loss analysis could be extended to the complete device stack, allowing the optimization of other material layers in the perovskite subcell and the evaluation of the impact of the Si surface on the efficiency of the 2T device.

Measuring Degradation and Improving Long-Term Stability

As described above in June 2016, we encapsulated six perovskite solar cells in three different packages at D2 Solar using a butyl rubber edge seal, ethylene vinyl acetate encapsulation and two sheets of 6”x6” glass. During a 1000 hour 85°C 85% humidity damp heat test, one of the packages failed, resulting in failure of it solar cells. The other two packages performed well and the efficiency of it solar cells actually improved by 10-20 %. Over the last year we have been preparing to test a much larger collection of cells and determine why the efficiency improved slightly with time. We have also begun preparation for measuring light-induced degradation.

In the last couple of months of the project we began depositing the perovskite solar cells on 2 x 2” glass substrates that also serve as encapsulation. The thin film electrodes are deposited on the glass and run out to the edge of the package. Another piece of glass is attached to the first piece of glass with butyl rubber edge seals. The top piece of glass is smaller than the first one so that the electrodes are exposed. This design eliminates the need to run a metal ribbon through the rubber edge seal and should substantially reduce leakage.

We have found that when we use Surlyn as an encapsulant to fill the space between the solar cell, the edge seal and the two sheets of glass, the solar cells do not survive thermal cycling because this polymer is too stiff and can pull off the electrode when it expands and contracts. When we use EVA, the encapsulant used in most solar panels, the packages survive 200 cycles between -40°C and 85°C. The details of this study have been submitted for publication and can be provided, but will not be covered further here since most of the thermal cycling research was supported by another grant. We do not see any signs of reaction between EVA and the parts of our solar cell that are covered with an ITO electrode, but we do see that EVA causes the perovskite to degrade where it is not covered with ITO. We suspect that the acetic acid that can be released from EVA attacks the perovskite. Since we do not want to rely completely on the ITO to protect the perovskite for 25 years, we are going to tried other encapsulants, such as polyolefins, that might be less chemically reactive. In the last month of the project, we found that polyolefin is much less reactive with the perovskite and consider it to be our best option for encapsulating perovskite solar cells.

We have noticed that thermal degradation tends to occur underneath the silver gridlines that improve the conductivity of the top indium tin oxide electrode. In another project supported by the BAPVC, we have also noticed using thermal imaging that perovskite solar cells have a tendency to develop shorts underneath the metal gridlines when operated in reverse bias. At first it was very surprising to us the silver had any influence on the perovskite solar cell given that it was separated from the other layers by an ITO layer that we thought was impermeable. To better understand the problem, we used XPS depth profiling and also pealed the top ITO layer from aged devices so that we could examine the damaged perovskite layer. It quickly became apparent that the halogens are able to go through the fullerenes, ALD SnO_2 and the ITO to react with the metal and that the silver can go in the other direction to react with the perovskite. We think that if the reaction is allowed to run long enough, a high density of iodine vacancies forms in the perovskite before they coalesce to form voids that are easily detected in a scanning electron microscope. This data has revealed that our ITO electrodes are far

more permeable than we once thought they were. In the future will will develop electrodes with less permeability at the grain boundaries and use diffusion barriers.

We have acquired a weatherometer to measure light-induced degradation. This tool has xenon lamps that can expose a shelf with an area 0.5 m^2 to one-sun illumination. We have also setup a 32-channel source-measure unit controlled by LabView and the electrical connections to monitor the performance of 32 packaged solar cells during testing. We only had time to run one round of testing in the summer of 2017. The solar cells lost 20-50 % of their efficiency after 1500 hours of one-sun illumination at at 55°C. We can see that the perovskite films change color dramatically where they are not covered by indium tin oxide and that the color change works its way inwards from the edge. It is for this reason that we switched to the polyolefin encapsulant.

Conclusions:

An ALD or pulsed-CVD processed SnO_2/ZTO window layer has enabled the successful fabrication of perovskite solar cells with high efficiency and improved stability. These vapor processes produces a compact, conformal, uniform, and highly transparent SnO_2/ZTO bilayer with efficient hole-blocking ability and sputter buffer layer properties, allowing for 1 cm^2 devices with no pinholes. These devices have the thermal and ambient stability to be further sealed with industry standard encapsulation such as EVA and glass. In addition to being made as single-junction devices on glass, the same devices were fabricated on silicon solar cells with planar front surfaces to form two-terminal tandems. When the perovskite cells were coupled with silicon heterojunction bottom cells with an excellent rear reflector and a-Si:H and ITO layers adjusted for the exclusively infrared spectrum, the resulting tandem reached an efficiency of 23.6% with no hysteresis and stable maximum power over more than 30 minutes under illumination. This efficiency is well beyond that of both sub-cells, beyond that of the record single-junction perovskite cell, and approaching that of the record single-junction silicon cell. Performance-loss simulations suggest the efficiency can be increased further by widening the bandgap of the perovskite and reducing front-surface reflection, which will enable both higher matched current densities and higher voltage.

We came tantalizingly close to accomplishing the aggressive project goal of achieving a 25% power conversion efficiency. We developed a commercially relevant packaging method for perovskite solar cells and then passed two of the most important industry standard reliability tests- the 1000 hour damp heat test at 85°C and 85% humidity and the temperature cycling test. We have not yet observed adequate stability under illumination, but have a great infrastructure in place for assessing light -induced stability that will allow us to address this issue in the future.

Budget and Schedule: Provide information on the project budget, including federal share, cost share, and amounts spent and unspent, along with an explanation for any

deviations from the spend plan. Provide information on the budget period schedules, including start dates, end dates, and any modifications, along with an explanation for any schedule modifications.

Lenny and Dana: We will complete this section before the final deadline.

Path Forward:

Mike McGehee, Zach Holman and Stacey Bent recently received a PVRD2 award to continue research on making perovskite-silicon tandems. Over the next three years we will try to achieve 30% power conversion efficiency while passing the important stability tests. Companies that have requested meetings with us to talk about the research include First Solar, SunPower, DuPont, Tesla, Exxon, EPRI, Oxford PV, BASF, Hunt Energy, Schlumberger and Total. There is a high level of interest amongst several current and former members of our research groups to startup a company to commercialize the technology.

Patents applications being processed

1. "Multijunction Perovskite/Crystalline Silicon Solar Cell with Tunnel Junction," USA Provisional 62/086,785
2. "Sputtered ITO Electrode Enabled by Doped Nanoparticle Buffer Layer for Improved Thermal and Environmental Stability of Semi-Transparent and Tandem Perovskite Solar Cells," Stanford Docket: 15-360.
3. "Metal Oxide Buffer Layers Deposited through Atomic Layer Deposition and Chemical Vapor Deposition to Stabilize Perovskite Solar Cells and Enable Sputtered Electrodes," Stanford Docket: 16-259.

References: List literature references cited in the report, using the format provided in RPPR Attachment 3.